MOLECULAR SIMULATION
2021, VOL. 47, NO. 17, 1391–1401
https://doi.org/10.1080/08927022.2021.1975038

Taylor & Francis
Taylor & Francis Group

Where is the hydrodynamic limit?

J. S. Hansen

"Glass and Time", IMFUFA, Department of Science and Environment, Roskilde University, Roskilde, Denmark

ABSTRACT

In this paper, the classical hydrodynamic theory is compared to molecular dynamics simulation data using two different dynamical modes, namely, the transverse and longitudinal modes. The comparison is based on the dynamics of the equilibrium fluctuations for four different systems, the Lennard-Jones system, model liquids for butane, toluene, and water. Using an error estimator limit of 1%, it is found that for the transverse dynamics the classical hydrodynamic theory holds down to 5–14 nm depending on the fluidic system. For the longitudinal dynamics, this characteristic length scale is approximately doubled. From the dispersion relations, it is furthermore concluded that classical hydrodynamics qualitatively accounts for the dominating processes at even lower length scales.

ARTICLE HISTORY
Received 16 March 2021
Accepted 24 August 2021

1. Introduction

Hydrodynamics describes the dynamics of fluids through macroscopic quantities like mass density, streaming velocity and energy [1, 2]. The fundamental assumption in hydrodynamics is that the quantities vary sufficiently smoothly in both time and space such that they can be treated mathematically as field variables; this is known as the continuum hypothesis [3]. The continuum hypothesis is not strictly true. Consider, for example, the mass density, $\rho_{\mathcal{V}}$, in some fixed fluid volume $\mathcal{V}$. In the no-flow situation hydrodynamics predicts that the mass density is a constant with respect to time, however, from a microscopic point of view $\rho_{\mathcal{V}}$ must fluctuate as molecules enter and exit $\mathcal{V}$ due to thermal motion. These fluctuations are not experienced on larger scales and usually not included in the hydrodynamic description as the intrinsic molecular nature of fluids is not considered or indeed not even defined. Hydrodynamics is therefore traditionally associated with physics on the macroscopic length scale [3].

The hydrodynamic theory has been extended to model the thermal fluctuations, for example, through the stochastic forcing method [2, 4, 5]. Here a zero-mean stochastic term is added to the system fluxes, and the hydrodynamic equations describing the fluid quantities become stochastic differential equations analogous to the Langevin equation. Upon averaging over an ensemble of independent initial conditions we recover the standard equations, but where the field variables are now ensemble averaged quantities. This stochastic forcing is founded in Onsager's famous regression hypothesis [6] and since the dynamics then includes the microscopic thermal fluctuation the theory may be considered as a microscopic theory. However, this does not address the fundamental question whether hydrodynamics is an appropriate description on the microscopic scale, that is, if the fundamental physics relevant on the macroscopic length scale is also present, and perhaps even dominant, in the microscopic regime.

It is important to recall that hydrodynamics is based on a set of balance equations and a set of constitutive relations that relate the system fluxes with the system forces [7]. The constitutive relations are models and hydrodynamics is therefore never exact, not even on large scales, but by definition an approximation to the real world. The statement that hydrodynamics "fails" on the microscopic scale is therefore strictly not meaningful, at least not without specifying what defines failure. How well the theory approximate the true hydrodynamics also depends to the specific system we consider and the exact dynamical phenomenon we study.

Furthermore, we must be clear on what exactly constitutes (or defines) a hydrodynamic theory. Here *classical* hydrodynamic theory provides the dynamics for mass, linear momentum, and energy densities and the constitutive relations are all based on linear models with constant scalar coefficients. This implies that we only model homogeneous and isotropic systems with symmetric stress in the limit of zero system forces. This leads to the well-known mass continuity, Navier-Stokes, and heat transport equations. The classical hydrodynamic theory has naturally been undergoing many extensions (besides the stochastic forcing method) to include different phenomena. For example, by including the coupling between the fluid linear and angular momenta [7–10], allowing for velocity slip boundary conditions [11–13], and nonlocal (generalized) transport coefficients [14, 15]. These phenomena are omnipresent, that is, extended hydrodynamics does not introduce any fundamental new physics, but the phenomena are usually safely ignored on the macroscopic length scales, however, not on the nanoscale. Modern theories have been applied with success to the extreme small scale, e.g. the generalized collective mode theory [16–18] and mode coupling theory, see for example Ref. [19].

For the reasons listed above a simple meaningful answer to the research question "Where is the hydrodynamic limit?" cannot be given unless we specify (i) what exactly we mean by

CONTACT J. S. Hansen jschmidt@ruc.dk

hydrodynamics, (ii) the system we study, (iii) what specific dynamical phenomenon we refer to, and (iv) some quantitative threshold value measuring the deviation between data and theory.

Naturally, this fundamental research question has been discussed thoroughly in the past, see e.g. Refs. [20–22], and due to its applicability classical hydrodynamics has been used as an underlying model to understand scattering experiments [23], small scale liquid state dynamics [19, 24], and nano-confined flow systems [25–27]. This paper seeks to contribute to the discussion and compare, directly, the classical hydrodynamic theory with molecular dynamics simulation data for four different model fluidic systems, namely, the standard Lennard-Jones system, butane in a high pressure liquid state, and toluene and water at ambient conditions. We will explore well-known hydrodynamic correlation functions in the non-confined equilibrium situation in order to avoid complicated effects related to molecular packing near surfaces, non-linear strain rate dependencies, alignment phenomena, etc., all effects that make a comparison with the theoretical predictions highly non-trivial. The exploration is based on a multi-scale study, thus, the characteristic length scale where phenomena not featured in the classical theory can be identified. The deviation between the data and the theory is measured via a mean square difference using an error threshold value of 1 %.

In the next section, the classical hydrodynamic correlation functions will be derived. Even if these are well-known [19, 28], the derivation ensures a clear definition of what exactly is here meant by classical hydrodynamics. The derivation also allows for some very important points to be highlighted. After this section, the fluid systems will be presented as well as the molecular dynamics simulation details. The final two sections will be devoted to results, discussion and conclusion.

2. The hydrodynamic correlation functions

In the classical treatment, the equilibrium dynamics is fully described by two correlation functions, namely, the transverse momentum current autocorrelation function and the longitudinal density autocorrelation function [24]. To first order in the fluctuations the momentum current autocorrelation function can be approximated with the velocity autocorrelation function, $C_{uu}^{\perp}$ [29], thus, the dynamics is given through the functions

$$C_{uu}^{\perp}(\mathbf{k}, t) = \frac{1}{V}\langle \widetilde{\delta u}_x(\mathbf{k}, t)\widetilde{\delta u}_x(\mathbf{k}, 0)\rangle \tag{1a}$$

$$C_{\rho\rho}(\mathbf{k}, t) = \frac{1}{V}\langle \widetilde{\delta\rho}(\mathbf{k}, t)\widetilde{\delta\rho}(-\mathbf{k}, 0)\rangle \tag{1b}$$

where $\widetilde{\delta u}_x$ and $\widetilde{\delta\rho}$ are the Fourier modes of the fluctuating part of the streaming velocity x-component and mass density, $\mathbf{k}$ is the wavevector perpendicular to the x-direction, $\langle\cdots\rangle$ indicates the average over an ensemble of independent initial conditions, and V is the system volume. The first undertaking is to derive the classical hydrodynamic expressions for $C_{uu}^{\perp}$ and $C_{\rho\rho}$.

We here follow Alley and Alder [28] and study the thermal kinetic energy density, $\rho\varepsilon$, rather than the total energy. Since we only explore relaxations in equilibrium we can ignore advection and viscous heating terms, and the three balance equations for mass, momentum, and energy densities read

$$\frac{\partial\rho}{\partial t} = -\nabla(\rho\mathbf{u}) \tag{2a}$$

$$\frac{\partial\rho\mathbf{u}}{\partial t} = -\nabla\cdot\mathbf{P} \tag{2b}$$

$$\frac{\partial\rho\varepsilon}{\partial t} = \frac{T\beta_V}{\rho}\frac{\partial\rho}{\partial t} - \nabla\cdot\mathbf{J}^{\varepsilon} \tag{2c}$$

where $\mathbf{u}$ is the streaming velocity, $\mathbf{P}$ is the pressure (or momentum flux) tensor, β_V is the thermal pressure coefficient, and $\mathbf{J}^{\varepsilon}$ the thermal kinetic energy flux tensor.

The hydrodynamic quantities ρ, $\mathbf{j} = \rho\mathbf{u}$, and $\rho\varepsilon$ are expressed in terms of the ensemble average denoted with a subscript av and the fluctuating part with pre-fix δ. To first order in the fluctuations, we have

$$\begin{aligned}\rho = \rho_{\text{av}} + \delta\rho, \quad \mathbf{j} = \rho_{\text{av}}\delta\mathbf{u}, \quad \text{and}\\ \rho\varepsilon = (\rho\varepsilon)_{\text{av}} + \delta(\rho\varepsilon).\end{aligned} \tag{3}$$

Notice that the derivatives of the average parts are all zero. Substitution into Equations (2a)–(2c) results in the balance equations for the fluctuations

$$\frac{\partial\delta\rho}{\partial t} = -\rho_{\text{av}}\nabla(\delta\mathbf{u}) \tag{4a}$$

$$\rho_{\text{av}}\frac{\partial\delta\mathbf{u}}{\partial t} = -\nabla\cdot\mathbf{P} \tag{4b}$$

$$\frac{\partial\delta(\rho\varepsilon)}{\partial t} = \frac{T\beta_V}{\rho_{\text{av}}}\frac{\partial\delta\rho}{\partial t} - \nabla\cdot\mathbf{J}^{\varepsilon} \tag{4c}$$

For homogeneous and isotropic fluids the linear constitutive relations (models) for the fluxes read [5, 28, 30]

$$\mathbf{P} = p_{\text{eq}}\mathbf{I} - \eta_\nu(\nabla\cdot\mathbf{u})\mathbf{I} - 2\eta_0\overset{os}{\nabla}\mathbf{u} + \delta\mathbf{P} \tag{5a}$$

$$\mathbf{J}^{\varepsilon} = -\frac{\lambda}{\rho_{\text{av}}c_V}\nabla\delta(\rho\varepsilon) + \delta\mathbf{J}^{\varepsilon} \tag{5b}$$

where p_{eq} is the equilibrium normal pressure, η_ν and η_0 are the bulk and shear viscosities, respectively, λ is the heat conductivity, c_V the specific heat capacity at constant volume, and $\mathbf{I}$ is the unit tensor. The trace-less and symmetric tensor, $\overset{os}{\nabla}\mathbf{u}$, is the strain-rate tensor. The last terms $\delta\mathbf{P}$ and $\delta\mathbf{J}^{\varepsilon}$ represent the stochastic forcing terms. For our purpose, it suffices to assume that these stochastic terms each have average of zero and are uncorrelated with the hydrodynamic quantities ρ, $\mathbf{u}$ and $\rho\varepsilon$.

Substitution of Equations (5a) and (5b) into Equations (4b) and (4c) gives the dynamical equations for the fluctuations to

first order

$$\frac{\partial \delta\rho}{\partial t} = -\rho_{\text{av}} \nabla \cdot \delta\mathbf{u} \tag{6a}$$

$$\rho_{\text{av}} \frac{\partial \delta\mathbf{u}}{\partial t} = -\nabla \delta p_{eq} + (\eta_v + \eta_0/3)\nabla(\nabla \cdot \delta\mathbf{u}) + \eta_0 \nabla^2 \delta\mathbf{u} - \nabla \cdot \delta\mathbf{P} \tag{6b}$$

$$\frac{\partial \delta(\rho\varepsilon)}{\partial t} = \frac{T\beta_V}{\rho_{\text{av}}} \frac{\partial \delta\rho}{\partial t} + \frac{\lambda}{c_V \rho_{\text{av}}} \nabla^2 \delta(\rho\varepsilon) - \nabla \cdot \delta\mathbf{J}^{\varepsilon} \tag{6c}$$

From Equations (1a) and (1b), it is seen that we look for the wavevector dependent dynamics. Then Fourier transforming Equations (6a)–(6c) we obtain

$$\frac{\partial \widetilde{\delta\rho}}{\partial t} = -i\rho_{\text{av}} \mathbf{k} \cdot \widetilde{\delta\mathbf{u}} \tag{7a}$$

$$\rho_{\text{av}} \frac{\partial \widetilde{\delta\mathbf{u}}}{\partial t} = -i\mathbf{k}\widetilde{\delta p}_{eq} - (\eta_v + \eta_0/3)\mathbf{k}(\mathbf{k} \cdot \widetilde{\delta\mathbf{u}}) - \eta_0 k^2 \widetilde{\delta\mathbf{u}} - i\mathbf{k} \cdot \widetilde{\delta\mathbf{P}} \tag{7b}$$

$$\frac{\partial \widetilde{\delta(\rho\varepsilon)}}{\partial t} = \frac{T\beta_V}{\rho_{\text{av}}} \frac{\partial \widetilde{\delta\rho}}{\partial t} - \frac{\lambda}{\rho_{\text{av}} c_V} k^2 \widetilde{\delta(\rho\varepsilon)} - i\mathbf{k} \cdot \widetilde{\delta\mathbf{J}}^{\varepsilon} \tag{7c}$$

2.1. Transverse relaxations

We can make a convenient choice for the wavevector, for example, $\mathbf{k} = (0, k_y, 0)$. We then obtain two equivalent and very simple dynamical equations for the x and z velocity vector Fourier modes. For example, for the x component, we have

$$\rho_{\text{av}} \frac{\partial \widetilde{\delta u}_x}{\partial t} = -\eta_0 k_y^2 \widetilde{\delta u}_x - ik_y \widetilde{\delta P_{yx}}. \tag{8}$$

The dynamical equation for the transverse velocity autocorrelation function, Equation (1a), can now be formed; multiplying Equation (8) by $\delta u_x(-k_y, 0)$ and ensemble averaging we get

$$\rho_{\text{av}} \frac{\partial C_{uu}^{\perp}}{\partial t} = -\eta_0 k_y^2 C_{uu}^{\perp}, \tag{9}$$

yielding an exponential relaxation

$$C_{uu}^{\perp}(k_y, t) = \frac{k_B T}{\rho_{\text{av}}} \, \mathrm{e}^{-\omega_0 t}, \tag{10}$$

in which ω_0 is the characteristic frequency having the dispersion relation $\omega_0 = \eta_0 k_y^2/\rho_{\text{av}}$. Thus, the transverse velocity autocorrelation function features a single process, in this case, it is diffusion of linear momentum. It does not include the presence of visco-elastic shear waves at small times and length scales [31–33].

From the frequency ω_0, we can define a characteristic decay time for a given wavevector as

$$\tau(k_y) = 2\pi\rho_{\text{av}}/(\eta_0 k_y^2). \tag{11}$$

Bocquet and Charlaix [34] argued that if τ is larger than the internal fluid stress relaxation time, τ_s, then the hydrodynamic model is satisfactory, that is, if

$$\tau > \tau_s \text{ implying } k_y < k_{BC} = \sqrt{\frac{2\pi\rho_{\text{av}}}{\eta_0 \tau_s}}. \tag{12}$$

Hansen et al. [29] suggested that τ_s can be found from the decay of the stress autocorrelation function. For example, τ_s is in order of 10 psec. for water at ambient conditions and we get $k_{BC} \approx 0.09$ Å^{-1}, corresponding to a characteristic wavelength of around 7 nm.

2.2. Longitudinal relaxations

We now return to the expression for the density autocorrelation function $C_{\rho\rho}$. In Equation (7b), the pressure is eliminated using the fundamental assumption of local thermodynamical equilibrium, that is,

$$\widetilde{\delta p}_{eq} = \frac{1}{\rho_{\text{av}} \beta_T} \widetilde{\delta\rho} + \frac{\beta_V}{\rho_{\text{av}} c_V} \widetilde{\delta\rho\epsilon}, \tag{13}$$

where β_T is the isothermal compressibility. For our choice of wavevector, Equations (7a)–(7c) then read

$$\frac{\partial \widetilde{\delta\rho}}{\partial t} = -i\rho_{\text{av}} k_y \widetilde{\delta u}_y \tag{14a}$$

$$\frac{\partial \widetilde{\delta u}_y}{\partial t} = -\frac{ik_y}{\rho_{\text{av}}^2 \beta_T} \widetilde{\delta\rho} - \nu_l k_y^2 \widetilde{\delta u}_y - \frac{ik_y \beta_V}{c_V \rho_{\text{av}}^2} \widetilde{\delta\rho\epsilon} - \frac{ik_y}{\rho_{\text{av}}} \widetilde{\delta P}_{yy} \tag{14b}$$

$$\frac{\partial \widetilde{\delta\rho\epsilon}}{\partial t} = -iT\beta_V k \widetilde{\delta u}_y - \kappa k_y^2 \widetilde{\delta\rho\epsilon} - ik_y \widetilde{\delta J}_y^{\epsilon} \tag{14c}$$

Here $\kappa = \lambda/c_V\rho_{\text{av}}$ and $\nu_l = (\eta_v + 4\eta_0/3)/\rho_{\text{av}}$ is the longitudinal kinematic viscosity. We see that the y velocity component couples to the density and energy fluctuations. From Equations (14a)–(14c), we can form nine correlation functions, e.g. the density–density, $C_{\rho\rho}$, density-velocity, $C_{\rho u}$, and density–energy $C_{\rho e}$, correlation functions can be defined by multiplying Equation (14a) with $\delta\rho(-k_y, 0)$, $\delta u_y(-k_y, 0)$, and $\delta\rho\varepsilon(-k_y, 0)$, respectively, and ensemble averaging. The dynamics of the nine correlation functions can be written in a compact matrix notation

$$\frac{\partial}{\partial t}\begin{pmatrix} C_{\rho\rho} & C_{\rho u} & C_{\rho e} \\ C_{u\rho} & C_{uu} & C_{ue} \\ C_{e\rho} & C_{eu} & C_{ee} \end{pmatrix} = -\begin{pmatrix} 0 & i\rho_{\text{av}} k_y & 0 \\ \frac{ik_y}{\rho_{\text{av}}^2 \beta_T} & \nu_l k_y^2 & \frac{ik_y \beta_V}{c_V \rho_{\text{av}}^2} \\ 0 & i\beta_V k_y & \kappa k_y^2 \end{pmatrix} \cdot \begin{pmatrix} C_{\rho\rho} & C_{\rho u} & C_{\rho e} \\ C_{u\rho} & C_{uu} & C_{ue} \\ C_{e\rho} & C_{eu} & C_{ee} \end{pmatrix}, \tag{15}$$

where $\cdot$ represents the standard matrix product. The coefficient matrix is referred to as the hydrodynamic matrix. It can be shown that the hydrodynamic matrix always has one real valued eigenvalue and two complex conjugated eigenvalues

$$\omega_1 = D_T k_y^2 + \mathcal{O}(k_y^4) \tag{16a}$$

$$\omega_{2,3} = \pm i c_s k_y + \Gamma k_y^2 + \mathcal{O}(k_y^3) \tag{16b}$$

where

$$c_s^2 = \frac{\gamma}{\rho_{\mathrm{av}}\beta_T}, \quad D_T = \frac{\lambda}{\rho_{\mathrm{av}}c_p} \quad \text{and} \quad \Gamma = \frac{1}{2}\left(\frac{\gamma-1}{\gamma}\kappa + \nu_l\right) \tag{17}$$

are the adiabatic speed of sound, thermal diffusivity, and sound attenuation coefficient, respectively, and $\gamma = c_p/c_V$, c_p being the specific heat capacity at constant pressure. Notice, that in the standard treatment [19], one truncates the eigenvalues, Equations (16a), after second order, thus, it is assumed *apriori* that the hydrodynamic description fails for larger wavevectors. Following the standard treatment, the solution for the density–density correlation function then reads to second order in wavevector

$$C^N_{\rho\rho}(k_y, t) = \frac{C_{\rho\rho}(k_y, t)}{C_{\rho\rho}(k_y, 0)} = \frac{1}{\gamma}\left[(\gamma-1)\,\mathrm{e}^{-D_T k_y^2 t} + \mathrm{e}^{-\Gamma k_y^2 t}\cos(c_s k_y t)\right]. \tag{18}$$

Thus, according to the classical hydrodynamic predictions the density autocorrelation function features a diffusive thermal damping process governed by D_T, this is the Rayleigh process, and a wave propagation process with speed c_s and damping coefficient Γ, this is referred to as the Brillouin process. All other longitudinal correlation functions are governed by the same two processes, and we need only to consider $C_{\rho\rho}$.

3. Molecular dynamics simulations

The hydrodynamic correlation functions $C^{\perp}_{uu}$ and $C_{\rho\rho}$ are evaluated for four different model fluidic systems: (i) the standard Lennard-Jones (LJ) system, (ii) butane, (iii) toluene and (iv) water. For the Lennard-Jones system, two different state points are explored, whereas for systems (ii)–(iv) a single liquid state-point is used. The choice of fluid systems then covers fluids composed of point mass particles, linear, ring structured and polar molecules.

The molecular dynamics simulations are carried out using the author's software package [35] and the GPU-based software package Roskilde University MD (RUMD) [36]. Both packages use the same underlying force field; see details in the software documentation. Force field parameters are based on the MM2 and TrAPPE force field parameters [37, 38] and also the work by Weiner et al. [39]; parameter values are specified below. All the simulations are carried out in the standard NVT statistical ensemble using the Nosé-Hoover thermostat [40, 41] or a simple relaxation thermostat [42, 43]; the results presented here are independent of this choice. Periodic boundary conditions are used and the equations of motion are solved numerically by a leap-frog algorithm [42]. All systems are equilibrated and simulated using ten statistically independent initial conditions except for the largest water system where a single run was performed using RUMD.

The LJ system is simulated at two state points: $(T, \rho) = (1.121, 0.85)$ and $(T, \rho) = (3.0, 0.85)$, the former representing a liquid and the latter a super-critical fluid. For the LJ system we represent all quantities in usual dimensionless molecular dynamics units, see Ref. [42]. The LJ system is the most commonly used model for a fluid composed of structure-less point mass particles (atoms or molecules), for example, argon or methane. The number of particles simulated is 16,361 corresponding to a maximum wavelength of 26.8; if the LJ particle represents methane this corresponds to approximately 10 nm.

The butane molecule is a fully flexible version of the united atomic unit (UAU) Ryckaert–Belleman model [44]. Each hydrocarbon group is represented by an LJ particle with LJ parameters $\sigma = 3.9$ Å, m=14.5 g mol^{-1}, and $\epsilon/k_B = 72.1$ K. Again, the reader is referred to Ref. [42] for the LJ parameter details. The rigid covalent bonds and bond angles in the Ryckaert–Bellemans model are replaced by flexible interactions. The bonds all have same zero-force length of $l_b = 1.58$ Å and a spring constant $k_s = 317$ kcal mol^{-1} Å^{-2}. The zero force angle is 1.9 radians with a force constant $k_\theta = 124$ kcal mol^{-1} rad^{-2}; the non-symmetric cosine squared angle potential is applied. The original torsion potential and parameters from Ryckaert–Belleman are adopted [44]. The state point $(T, \rho) = (298.15\,\mathrm{K}, 592.6\,\mathrm{kg\,m^{-3}})$ chosen is near the boiling point and is well studied making comparisons with literature possible; the model viscosity is 0.18 ± 0.02 mPa s, which is in very good agreement with previous simulation data, see Daivis and Evans [45]. Two thousand molecules are simulated giving a maximum accessible wavelength of 6.9 nm.

For toluene a flexible UAU model is also adopted using same LJ parameters for all particles $\sigma = 3.675$ Å, m=13.143 g mol^{-1}, and $\epsilon/k_B = 60$ K. In the phenyl group the zero-force covalent bond lengths are set to $l_b = 1.4$ Å with a spring constant of $k_s = 431$ kcal mol^{-1} Å^{-2}. Zero force angles are 2.09 radians using a force constant $k_\theta = 139$ kcal mol^{-1} rad^{-2} in the cosine squared potential. For the Ryckaert–Bellemans torsion potential, one term is non-zero using force constant of $k_\phi = 15$ kcal mol^{-1} rad^{-2}; this ensures a sufficiently flat ring structure as well as keeping the methyl group in-plane with the ring. The methyl-phenyl bond length is $l_b = 1.5$ Å having the same spring force constant $k_s = 431$ kcal mol^{-1} Å^{-2}. At state point $(T, \rho) = (300\,\mathrm{K}, 879\,\mathrm{kg\,m^{-3}})$, the model features ambient pressure and a viscosity of 0.4 ± 0.1 mPa s. This is in agreement with the all atom model by Fioroni and Vogt [46]. Four thousand molecules are simulated corresponding to a maximum wavelength of 8.8 nm.

Finally, the water model is given by the flexible SPC/Fw model [47, 48]. The Coulomb interactions where calculated using the shifted force method, see Refs. [49, 50]. Two different system sizes where simulated, one with 2000 molecules and one with 33×10^3 molecules. The larger system was simulated with only one production run using RUMD making it possible to probe the largest wavelength of approximately 10 nm. The system state point is $(T, \rho) = (298.15\,\mathrm{K}, 995\,\mathrm{kg\,m^{-3}})$ giving an ambient pressure. See Wu et al. [47] for more details on how this model predicts the thermodynamical and hydrodynamical coefficients.

4. Results

4.1. Transverse dynamics

First, we focus on the transverse dynamics and to this end we will need the viscous properties at zero wavevector. The zero wavevector Irving-Kirkwood pressure tensor is [51, 52]

$$\mathbf{P}(t) = \frac{1}{V}\left[\sum_i m_i \mathbf{v}_i\mathbf{v}_i + \sum_i \sum_{j>i} \mathbf{r}_{ij}\mathbf{F}_{ij}\right], \tag{19}$$

where $\mathbf{r}_{ij} = \mathbf{r}_i - \mathbf{r}_j$ and $\mathbf{F}_{ij}$ is the force acting on molecule i due to j. Note that as the pressure tensor is defined in terms of molecular quantities it is not symmetric for systems (ii)–(iv), but has an anti-symmetric part as $\mathbf{r}_{ij}$ and $\mathbf{F}_{ij}$ are not in general parallel vectors. The time-dependent viscosity is found from the standard Green-Kubo integral [42]

$$\eta(t) = \frac{V}{k_B T}\int_0^t \langle \overset{os}{P}_{xy}(t') \overset{os}{P}_{xy}(0)\rangle \, \mathrm{d}t', \tag{20}$$

where $\overset{os}{P}_{xy}$ is the symmetric part of the shear pressure tensor xy component. The zero-frequency shear viscosity is then found from the limit $\eta_0 = \lim_{t\to\infty}\eta(t)$. In practice η is calculated using all shear pressure tensor components to improve the statistics. Table 1 lists η_0 for all model systems studied.

The fluid internal stress relaxation time τ_s is defined as in Ref. [29], that is, it is the minimum time where $\eta(t) = \eta_0$, or equivalently, τ_s is determined by the fully decayed stress correlation function. Naturally, due to the statistical uncertainties this criterion is somewhat ambiguous. As an example, η is plotted in Figure 1 for butane and the estimated relaxation time indicated. Table 1 lists the decay times for all systems.

An alternative choice for the stress relaxation time is the Maxwell time $\tau_M = \eta_0/G_\infty$, where G_∞ is the modulus of rigidity. Using Maxwell's visco-elastic model we obtain the general relation $\tau_M < \tau_s$, hence, the Maxwell time is lower than the time it takes the stress to fully decay. Also, using τ_M in turn implies that the Bocquet–Charlaix wavevector k_{BC} will be relatively large compared to using τ_s; we will address this point below.

Having the viscosities and the decay times the characteristic wavelength obeying the Bocquet–Charlaix criterion can be estimated, see Table 1. Thus, for butane, toluene and water, we obtain characteristic length scales of 3.2, 5.5 and 6.9 nm, respectively. If one applies the LJ length scale parameter for methane $\sigma = 3.7$ Å we get approximately 2 and 2.2 nm for the super-critical and liquid state points, respectively.

To evaluate the correlation functions the following microscopic definitions for density and streaming velocity are used [19, 29]

$$\widetilde{\rho}(\mathbf{k}, t) = \sum_i m_i \, \mathrm{e}^{-i\mathbf{k}\cdot\mathbf{r}_i} \tag{21a}$$

$$\widetilde{\mathbf{u}}(\mathbf{k}, t) = \frac{1}{\rho_{\mathrm{av}}}\sum_i m_i \mathbf{v}_i \, \mathrm{e}^{-i\mathbf{k}\cdot\mathbf{r}_i} \tag{21b}$$

where m_i, $\mathbf{r}_i$, and $\mathbf{v}_i$ are the mass, centre-of-mass, and centre-of-mass velocity. From this $C^{\perp}_{uu}$ and $C_{\rho\rho}$ can be calculated directly from their definitions, Equations (1a) and (1b).

A direct comparison between the theory and simulation data for $C^{\perp}_{uu}$ can be achieved using η_0 from Table 1 in Equation (10). That is, no fitting is performed. Figure 2 shows the transverse velocity autocorrelation function for the four systems (using the LJ liquid state point $(T, \rho) = (1.121, 0.85)$). The filled circles connected with lines are data points and the punctured lines represent the hydrodynamic predictions. For the LJ liquid the relaxation is very well described by the classical hydrodynamic theory when $k_y = 0.23$; even for $k_y = 0.47$ the agreement is good. Notice that these two wavevectors fulfils $k_y < k_{BC}$. For toluene $k_{BC} = 0.11$ Å^{-1}; the lowest wavevector studied for this system is 0.07 Å^{-1}, thus, $k_y \lesssim k_{BC}$. Clearly, the agreement is less satisfactory compared to wavevectors significantly lower than k_{BC}.

To quantify the discussion, we define the error estimator, err, by

$$\mathrm{err}(k_y) = \frac{\int\left[C_{\mathrm{MD}}(k_y, t) - C_{\mathrm{pred}}(k_y, t)\right]^2 \mathrm{d}t}{\int C^2_{\mathrm{pred}}(k_y, t)\,\mathrm{d}t}, \tag{22}$$

where C_{MD} is the correlation function obtained from simulations and C_{pred} the prediction from the theory. To avoid including the spurious fluctuations in data at long times (resulting in larger values for the error estimator) a Hann window is applied. For the LJ system err ≈ 5 % for $k_y \approx k_{BC}$, and err ≈ 0.5% for $k_y = 0.47$. For butane we observe the same tendency: at $k_y \approx k_{BC}$, the error estimator is around 5 % and for $k_{BC}/2 \approx k_y = 0.09$ Å^{-1} we get err ≈ 1%; this threshold value is used in this work to indicate a good agreement between data and theory. This result indicates that τ_s estimated above from the stress autocorrelation function will not account for the full stress relaxation. This may be due to persistent, but small magnitude system stresses not visible within errors in data. As stated above, we generally have that $\tau_M < \tau_s$, that is, using τ_M will lead to increasing values for k_{BC} resulting in an even larger error, hence, the Maxwell time is not the appropriate relaxation time.

As the wavevector increases the transverse velocity autocorrelation function features anti-correlations. As mentioned above, these anti-correlations are finger-prints of visco-elastic behaviour and calls for an alternative constitutive model than Newton's law of viscosity, e.g. the Maxwell model [30]. The focus of this paper is the classical theory and we will not seek to discuss other models here.

It is informative to explore the corresponding mechanical spectrum, $\widehat{C}^{\perp}_{uu}(k_y, \omega)$. To obtain the theoretical expression we simply Fourier–Laplace transform Equation (10), giving the imaginary part of the spectrum

$$\mathrm{Im}\left[\widehat{C}^{\perp}_{uu}(k_y, \omega)\right] = \frac{k_B T}{\rho_{\mathrm{av}}}\frac{\omega}{\omega_0^2 + \omega^2}. \tag{23}$$

Thus, the spectrum is predicted to show a maximum at the peak frequency $\omega_{\mathrm{peak}} = \omega_0 = \eta_0 k_y^2/\rho_{\mathrm{av}}$. The peak frequency shifts proportional with k_y^2, and this defines the dispersion relation for the transverse hydrodynamic as mentioned above. Figure 3 plots the peak frequency as a function of wavevector for the four systems. The predictions is also plotted (punctured lines) using η_0 from Table 1.

Table 1. Parameters and transport properties for the different model fluids. The shear viscosity, η_0, and the stress relaxation time, τ_s, are calculated from the stress relaxation function, Equation (20). The ratio of heat capacities γ, thermal diffusivity, D_T, attenuation coefficient, Γ, and speed of sound, c_s, are fitted values from smallest wavevectors studied. For water a single large system size production run was performed and the statistical uncertainty therefore not listed.

System	η_0 [mPa s]	τ_s [psec]	$2\pi/k_{BC}$ [nm]	γ	c_s [m s^{-1}]	D_T [10^{-7} m^2 s^{-1}]	Γ [10^{-7} m^2 s^{-1}]
LJ[a]	2.15 $\pm$ 0.3	0.4	2.5	1.62 $\pm$ 0.03	8.98 $\pm$ 0.07	3.5 $\pm$ 0.2	2.9 $\pm$ 0.2
LJ[b]	2.72 $\pm$ 0.07	2	6	–	–	–	–
Butane	0.18 $\pm$ 0.02	6	3.2	1.70 $\pm$ 0.06	1273 $\pm$ 12	2.1 $\pm$ 0.1	3.27 $\pm$ 0.08
Toluene	0.4 $\pm$ 0.1	10	5.5	2.3 $\pm$ 0.2	1440 $\pm$ 28	2.4 $\pm$ 0.4	3.7 $\pm$ 0.5
Water	0.75 $\pm$ 0.01	10	6.9	3.4	1209	8	6

[a]Reduced MD units. Super-critical state point (T, ρ)=(3.0, 0.85). [b]Reduced MD units. Liquid state point (T, ρ)=(1.121, 0.85).

At low wavevectors the theory correctly predicts the dispersion relation for the peak frequency. However, over the entire wavevector interval the data shows a non-linear dependency with respect to the wavevector squared and varies in a continuous concave fashion. Even for the LJ system at small wavevectors (the inset in Figure 3(a)), the concave behaviour appears to be present, however, this cannot be resolved within statistical uncertainty. In terms of the hydrodynamic frame work, the concave behaviour indicates that the viscosity decreases as function of k_y. This is in agreement with the results from generalised hydrodynamics wherein the non-local viscosity kernel decreases as function of k_y [14].

It is interesting to note, again within statistical uncertainty, that the wavevector squared dependency is fulfilled for relatively large wavevectors compared to the discussion above. For example, for butane, the peak frequency is predicted to be $\omega_{\text{peak}} = 1.8$ THz at $k_y = 0.27$ Å^{-1}, which is in agreement with data. However, here the time-dependent correlation function featured visco-elastic effects and one can based on this argue that the theory fails. Here the dispersion plot is interpreted such that the momentum diffusion is the dominating process behind the relaxation phenomenon as correctly predicted by the theory; even though at these small length scales other processes also come in to play.

4.2. Longitudinal dynamics

The protocol used in the comparison of the longitudinal dynamics is different from the transverse dynamics as not all thermodynamic and transport coefficients are calculated from independent methods enabling a direct comparison. Therefore, the theoretical prediction of the density autocorrelation function, Equation (18), is fitted to simulation data using γ, D_T, Γ and c_s as fitting parameters; results of this fitting can be found in Table 1 for the systems' lowest wavevector. Notice that the LJ system is studied at a super-critical state point in order to confirm, at least some of, the fitted parameter values with values available in the literature.

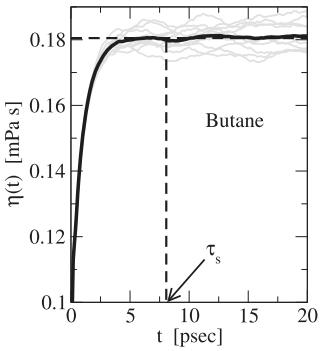

Figure 1. Running integral for the stress relaxation, Equation (20), for the model butane system. All 10 independent simulation runs are shown as grey lines and the sample mean as black line. Horizontal punctured line indicates the viscosity and the vertical punctured line the corresponding estimated stress relaxation time τ_s.

Figure 4 shows the density autocorrelation function for the two lowest wavevectors. Symbols connected with lines represent data and punctured lines are best fits of Equation (18) to data. From this we see that both the Rayleigh and Brillouin processes predicted by the classical theory are indeed also present on the nano-scale. The error estimator for the lowest wavevectors are also given in Figure 4.

For the LJ system Mairhofer and Sadus [53] found $\gamma \approx 1.6$ and $c_s = 8.7$ from their statistical mechanical definitions. These values are in agreement with the fitted values and this strongly indicates that the classical hydrodynamic regime is reached (within error) for $k_y = 0.23$. However, already at $k_y = 0.47$ the fitted values for γ and c_s are significantly different from Mairhofer and Sadus' values. From the results above for the transverse dynamics this indicates that the classical hydrodynamic limit is dependent on the specific dynamics we study. In particular, it means that the theory is less satisfactory for the longitudinal dynamics compared to the transverse dynamics at a given wavevector. Immediately, this leads to the question if this larger length scale pertain to the Rayleigh process or the Brillouin process.

First, we investigate the Rayleigh process from the so-called half-width dispersion relation. To do so, it is noted that the mechanical spectrum for the density autocorrelation function is directly related to the dynamic structure factor, S,

$$S(k_y,\omega) = \frac{\Delta S}{\gamma}\left[\frac{(\gamma-1)D_T k_y^2}{D_T^2 k_y^4+\omega^2} + \frac{(c_s^2 k_y^2+\Gamma^2 k_y^4+\omega^2)\Gamma k_y^2}{(c_s^2 k_y^2+\Gamma^2 k_y^4-\omega^2)^2+4\omega^2\Gamma^2 k_y^4}\right], \tag{24}$$

where ΔS is the pre-factor. The first term on the right-hand side is the Rayleigh process and the second term the Brillouin process. Equation (24) can be derived directly from the Fourier–Laplace transformation of Equation (18). As an example, Figure 5 shows the normalised dynamical structure factor for toluene at wavevectors $k_y = 0.07$ Å^{-1} and $k_y = 0.43$ Å^{-1}. The Rayleigh half-width peak is also illustrated here.

Classical hydrodynamics predicts that

$$\Delta\omega_{\text{Ra}} = D_T k_y^2, \tag{25}$$

and Figure 6 shows this dispersion relation. Symbols represent fit of Equation (18) to raw simulation data (filled

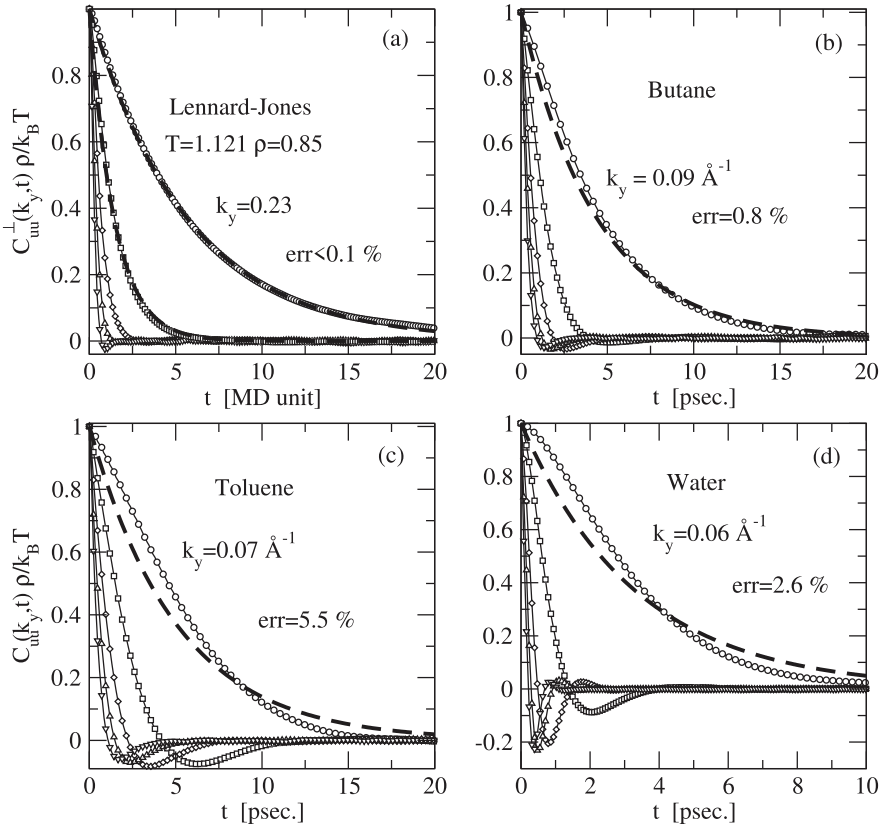

Figure 2. Transverse velocity autocorrelation function for different wavevectors. The wavevector shown for each system is the minimum wavevector studied; the other wavevectors are given by integer multiple of that: $2k_y$ (squares), $3k_y$ (diamonds), $4k_y$ (up-triangles), and $5k_y$ (down-triangles). The error estimator, err, pertains to the lowest wavevector and is defined in Equation (22). (a) LJ liquid at state-point $(\rho, T) = (0.85, 1.121)$. (b) Butane. (c) Toluene. (d) Water. The punctured lines are hydrodynamic predictions using the zero-wavevector zero-frequency shear viscosity. Note, for LJ the predictions for the two lowest wavevectors are shown.

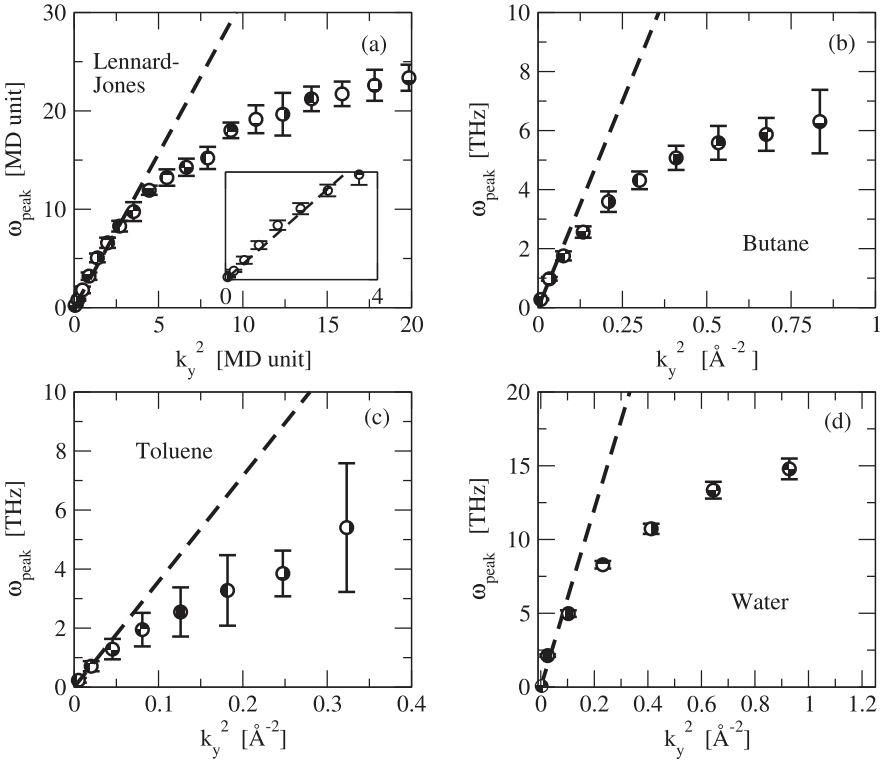

Figure 3. Peak frequency as a function of wavevector for the transverse dynamics. The filled circles represents simulation data and the punctured lines prediction from theory. Note, no fitting is performed.

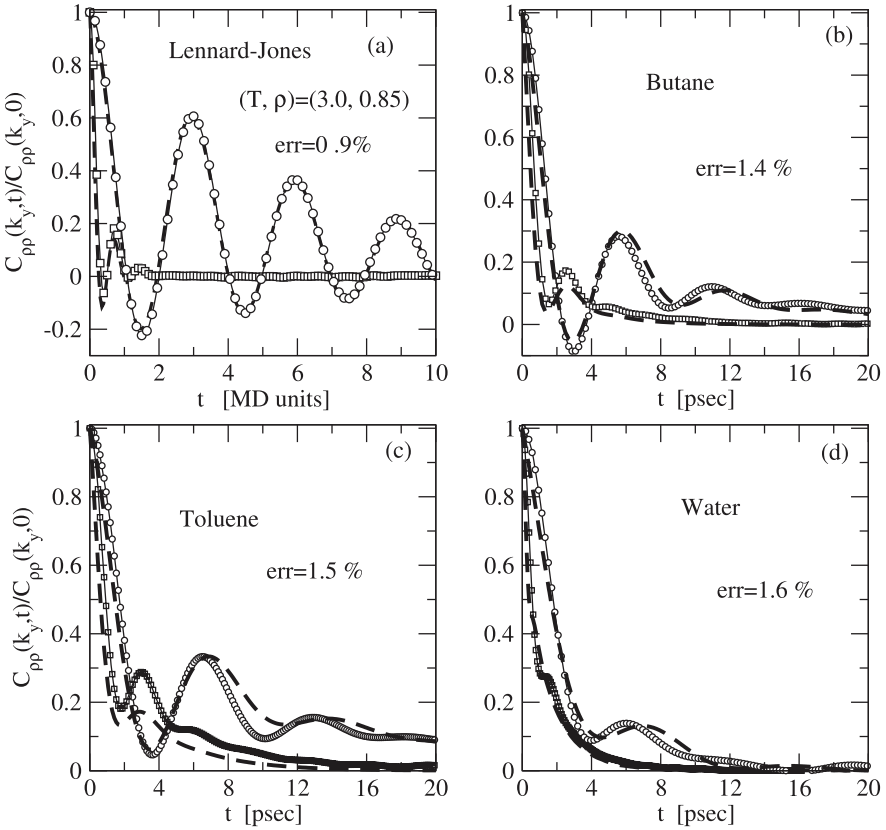

Figure 4. Density autocorrelation function for the two smallest wavevectors, see also Figure 2. (a) LJ super-critical fluid at state-point (T, ρ) = (3.0, 0.85), (b) butane, (c) toluene, and (d) water. Symbols connected with lines are data points and the punctured lines are best fit of Equation (18) to data. The error estimator are for the lowest wavevectors.

circles) or fit of Equation (24) to transformed data (open squares). In these fits the coefficient are allowed to be wavevector dependent, especially we have $D_T = D_T(k_y)$, and data point are then calculated using Equation (25). The punctured lines are predictions from Equation (25) using D_T found for the smallest wavevector, thus assuming this is sufficiently close to the limit value as $k_y \to 0$; this will be commented below. It can be seen that the fit of Equation (24) to transformed data result in relatively large uncertainties, and we therefore will not apply this method from hereon.

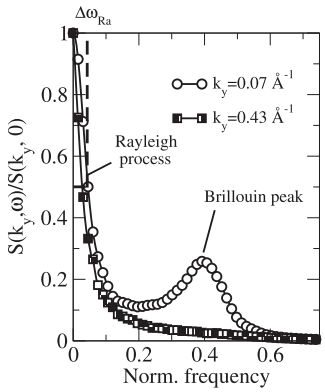

Figure 5. Dynamical structure factor for the model toluene liquid at two different wavevectors. The frequency is normalised with respect to the maximum spectrum frequency that includes the Brillouin process.

The predictions begin to deviate from data at lower wavevectors compared to the transverse case. For butane the predicted transverse dispersion relation agreed with data up to k_y = 0.27 Å^{-1} within statistical uncertainty, see Figure 3. In Figure 6, a deviation is observed above 0.18 Å^{-1}. This confirms the observation based on the fitted values of γ and c_s for the LJ super-critical fluid.

Recall, the prediction is based on the fitted value of D_T at lowest wavevector and the prediction will therefore always intersect origo and the first data point. For toluene and water the second data point deviates from the prediction and we can therefore only state that the hydrodynamic prediction fails for $k_y > 0.14$ Å^{-1} and $k_y > 0.12$ Å^{-1} for toluene and water, respectively. The actual lower limit is not accessible.

It is worth noting that the well-known de Gennes narrowing phenomenon [19] is seen for both the LJ and butane systems. For toluene the peak is not resolved within error, and for water not seen at all, at least not in the wavevector range studied here.

We then explore the Brillouin process, again via a dispersion relation. For larger wavevectors the Brillouin process becomes fast meaning that the superimposed oscillations are not clearly featured in the correlation function and thus is dominated by the monotonically decaying Rayleigh process.

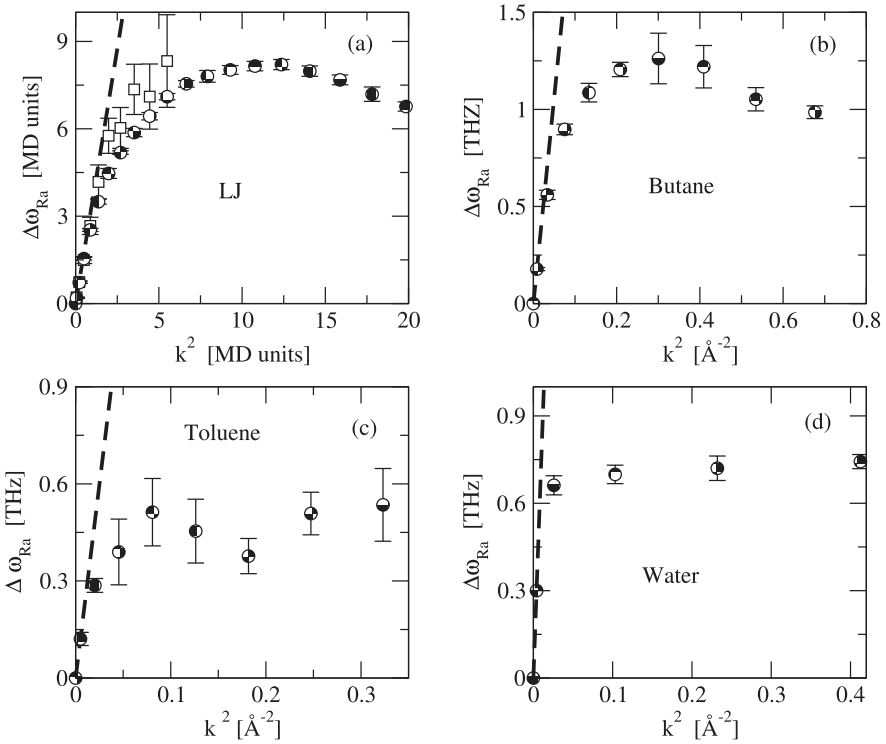

Figure 6. Dispersion relation for the Rayleigh process. (a) LJ super-critical fluid at state point (T, ρ) = (3.0, 0.85), (b) butane, (c) toluene and (d) water. Symbols are data points and the punctured lines are given by Equation (25) using the lowest wavevector value of D_T. Open squares are best of Equation (24) to Fourier-Laplace transformed data and filled circles best fit of Equation (18) to raw data.

Fitting Equation (18) with four parameters to such featureless data leads to a smaller error estimate, but clearly also an over-parametization and parameter sloppiness. One may attempt to extract the Brillouin process through the mechanical spectrum, Figure 5. For low wavevectors both processes are again clearly observed, however, as k_y increases the Brillouin peak may shift to higher frequencies and separate from the Rayleigh process, but the magnitude becomes small and the peak cannot be extracted within data noise levels. Only for the LJ and butane systems can the Brillouin process be extracted for larger wavevectors.

The dispersion relation studied for the Brillouin process is the peak frequency

$$\omega_{\text{peak}} = c_s k_y, \tag{26}$$

see Figure 5. Again, allowing the coefficients to be wavevector dependent and then using Equation (26) we arrive at the dispersion plot shown in Figure 7 for the LJ and butane systems. This is compared with the dispersion relation (punctured line) using the fitted value for c_s at lowest wavevector. The Brillouin dispersion relations, Figure 7, do not feature the so-called

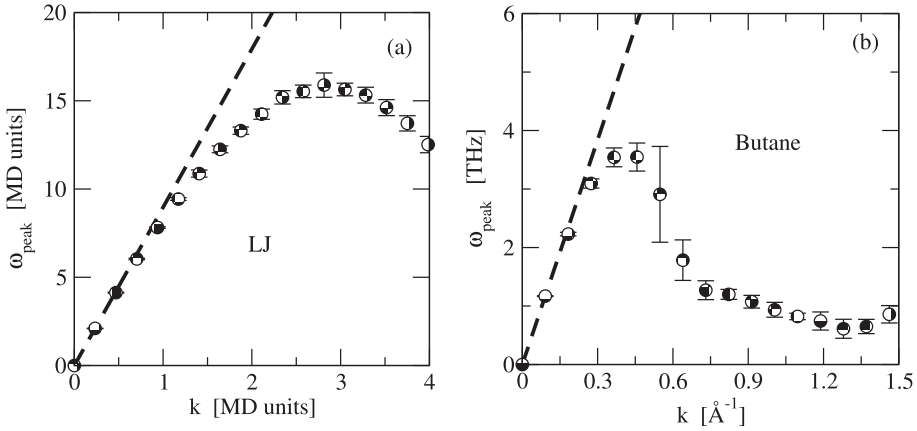

Figure 7. Dispersion relation for the Brillouin process. (a) LJ fluid at state-point (T, ρ) = (3.0, 0.85). (b) Butane. Symbols are data points and the punctured lines are given by Equation (26) using the fitted lowest wavevector value of c_s.

positive or negative dispersion relation [17, 19], at least not within statistical uncertainty; likely due to the specific state point chosen.

This dispersion plot shows the same wavevector threshold value as for the Rayleigh process, hence, the lowered threshold value does not pertain one specific longitudinal process. This is, perhaps, to be expected since both these processes are governed by the same system properties like heat conductivity and heat capacities.

5. Conclusion

First, the classical hydrodynamic prediction for the transverse velocity autocorrelation function was compared with data from molecular dynamics simulation. Here only one zero wavevector and zero frequency transport coefficient (the shear viscosity) is needed to make a direct comparison, that is, without any fitting. The agreement was quantified through a sum of squared deviations estimator denoted err, Equation (22). For the LJ and butane systems err is approximately 1 % for wavelength twice that of the Bocquet–Charlaix wavevector using the stress relaxation time τ_s. Accepting this one per cent error in the predictions and allowing for extrapolation the classical hydrodynamics is valid for $k_y < 0.09$ Å^{-1}, 0.057 Å^{-1}, and 0.045 Å^{-1} for the butane, toluene, and water, respectively. This corresponds to characteristic length scales from 7 to 14 nm. If one applies the LJ parameters for methane the minimum acceptable wavelength is around 5 nm in the liquid state.

For one per cent error the classical theory still do not qualitatively account for the temporal correlation seen in the data. For all systems a clear non-exponential decay is observed, however, from the error estimator these effects appear small compared the underlying momentum diffusion-driven exponential decay. This observation was confirmed by the transverse dispersion relation.

Secondly, a comparison between theory and data was also carried out for the longitudinal dynamics, specifically, through the density autocorrelation function. Due to the very many coefficients entering this part of the dynamics, the comparison was based on a fit of the prediction to data and the dispersion relations pertaining to the Rayleigh and Brillouin processes. Overall the agreement was found to be poor compared to the transverse dynamics at the same wavevector. Furthermore, the theory fails at the same threshold wavevector for both processes, hence, the poor agreement is not due to only one of the two mechanisms. Allowing a one per cent error the theory is valid at wavevectors below 0.23 for the LJ system corresponding to wavelength of 10.1 nm for methane, that is, approximately twice the threshold value of the transverse dynamics. It is here conjectured that this result is general, and that the classical hydrodynamic prediction for the longitudinal dynamics and under the one per cent threshold limit is valid for wavevectors $k_y < 0.045$ Å^{-1}, 0.024 Å^{-1}, and 0.023 Å^{-1} for the butane, toluene, and water, respectively. Importantly, the error estimator and threshold acceptance value is, of course, not uniquely defined.

Disclosure statement

No potential conflict of interest was reported by the author(s).

Funding

This work was supported by Villum Fonden [16515].

References

[1] Batchelor GK. An introduction to fluid dynamics. Cambridge: Cambridge University Press; 1967.
[2] Landau L and Lifshitz E. Fluid mechanics. 2nd ed. Amsterdam: Elsevier; 1987.
[3] Lautrup B. Physics of continuous matter. Bristol: Institute of Physics Publishing; 2005.
[4] Landau L and Lifshitz E. Statistical physics. 3rd ed. OXford: Pergmon Press; 1980.
[5] de Zárate J and Sengers J. Hydrodynamic fluctuations. Amsterdam: Elsevier; 2006.
[6] Onsager L. Reciprocal relations in irreversible processes. I.. Phys Rev. 37:1931;405–426.
[7] de Groot SR and Mazur P. Non-equilibrium thermodynamics. New York: Dover Publications; 1984.
[8] Cosserat E and Cosserat F. Sur la théorie de l'élasticité. Premier mémoire. Ann Toulouse. 10:1896;1–116.
[9] Bonthuis JD, Horinek D and Bocquet L, et al. Electrohydraulic power conversion in planar nanochannels. Phys Rev Lett. 103:2009;144503.
[10] Hansen JS, Dyre JD and Daivis PJ, et al. Nanoflow hydrodynamics. Phys Rev E. 84:2011;036311.
[11] Navier CLMH . Memoire sur les lois du mouvement des fluids. Memoires de l'Academic Royale des Sciences de l'Institut de France. 6:1823;389.
[12] Bocquet L and Barrat J-L. Hydrodynamic boundary conditions, correlation functions, and Kubo relations for confined fluids. Phys Rev E. 49:1994;3079–3092.
[13] Hansen J, Todd B and Daivis P. Prediction of fluid velocity slip at solid surfaces. Phys Rev E. 84:2011;016313.
[14] Hansen JS, Daivis PJ and Travis KP, et al. Parameterization of the nonlocal viscosity kernel for an atomic fluid. Phys Rev E. 76:2007;041121.
[15] Todd BD, Hansen JS and Daivis P. Nonlocal shear stress for homogeneous fluids. Phys Rev Lett. 100:2008;195901.
[16] de Schepper IM, Cohen EGD and Bruin C, et al. Hydrodynamic time correlation functions for a Lennard-Jones fluid. Phys Rev A. 38:1988;271–287.
[17] Bryk T, Mryglod I and Scopigno T, et al. Collective excitations in supercritical fluids: analytical and molecular dynamics study of "positive" and "negative" dispersion. J Chem Phys. 133:2010;024502.
[18] Bryk T, Mryglod I and Ruocco G. Non-hydrodynamic modes in viscoelastic behaviour of simple fluids. Phil Mag. 100:2020;2568–2581.
[19] Hansen JP and McDonald IR. Theory simple liquids. Amsterdam: Academic Press; 2006.
[20] Hilbert D. Mathematical problems. Bull Am Math Soc. 37:2000;407–436.
[21] McQuarrie DA. Statistical mechanics. New York (NY): Harper and Row; 1976.
[22] Bardos C, Golse F and Levermore D. Fluid dynamic limits of kinetic equations. I. Formal derivations. J Stat Phys. 63:1991;323–344.
[23] Bodensteiner T, Morkel C and Gläser W, et al. Collective dynamics in liquid cesium near the melting point. Phys Rev A. 45:1992;5709–5720.
[24] Boon J and Yip S. Molecular hydrodynamics. New York: Dover Publication; 1991.
[25] Koplik J, Banavar J and Willemsen J. Molecular dynamics of fluid flow at solid surfaces. Phys Fluid A. 1:1989;781–794.
[26] Travis KP, Todd BD and Evans DJ. Departure from Navier-Stokes hydrodynamics in confined liquids. Phys Rev E. 55:1997;4288–4295.
[27] Travis KP, Todd BD and Evans DJ. Poiseuille flow of molecular fluids. Phys A. 240:1997;315–327.

[28] Alley WE and Alder BJ. Generalized transport coefficients for hard spheres. Phys Rev A. 27:1983;3158–3173.
[29] Hansen J, Dyre J and Daivis P, et al. Continuum nanofluidics. Langmuir. 31:2015;13275–13289.
[30] Phan-Thien N. Understanding viscoelasticity: an introduction to rheology. Springer Verlag; Berlin: 2002.
[31] Frenkel J. Kinetic theory of liquids. Dover: Dover Publications; 1955.
[32] Yang C, Dove MT and Brazhkin VV, et al. Emergence and evolution of the k gap in spectra of liquid and supercritical states. Phys Rev Lett. 118:2017;215502.
[33] Bryk T, Mryglod I and Ruocco G, et al. Comment on "emergence and evolution of the k gap in spectra of liquid and supercritical states. Phys Rev Lett. 120:2018;219601.
[34] Bocquet L and Charlaix E. Nanofluidics, from bulk to interfaces. Chem Soc Rev. 39:2010;1073–1095.
[35] Hansen J. https://github.com/jesperschmidthansen/seplib
[36] Bailey NP, Ingebrigtsen TS and Hansen JS, et al. RUMD: a general purpose molecular dynamics package optimized to utilize GPU hardware down to a few thousand particles. SciPost Phys.. 3:2017;038.
[37] Allinger N. Conformational analysis. 130. MM2. A hydrocarbon force field utilizing V1 and V2 torsional terms. J Am Chem Soc. 99:1977;8127.
[38] Martin MG and Siepmann JI. Transferable potentials for phase equilibria. 1. United-atom description of n-alkanes. J Phys Chem B. 102:1998;2569–2577.
[39] Weiner S, Kollman P and Case D, et al. A new force field for molecular mechanical simulation of nucleic acids and proteins. J Am Chem Soc. 106:1984;765.
[40] Nosé S. A molecular dynamics method for simulations in the canonical ensemble. Mol Phys. 52:1984;255.
[41] Hoover WG. Canonical dynamics: equilibrium phase-space distributions. Phys Rev A. 31:1985;1695.
[42] Allen MP and Tildesley DJ. Computer simulation of liquids. New York (NY): Clarendon Press; 1989.
[43] Frenkel D and Smit B. Understanding molecular simulation. London: Academic Press; 1996.
[44] Ryckaert J-P and Bellemans A. Molecular dynamics of liquid alkanes. Faraday Discuss Chem Soc. 66:1978;95.
[45] Daivis PJ and Evans DJ. Transport coefficients of liquid butane near the boiling point by equilibrium molecular dynamics. J Chem Phys. 103:1995;4261.
[46] Fioroni M and Vogt D. Toluene model for molecular dynamics simulations in the ranges $298 < T(\mathrm{K}) < 350 \text{and} 0.1 < P(\mathrm{MPa}) < 10$. J Phys Chem B. 108:2004;11774.
[47] Wu Y, Tepper HL and Voth GA. Flexible simple point-charge water model with improved liquid-state properties. J Chem Phys. 124:2006;024503.
[48] Raabe G and Sadus RJ. Surface enhanced Raman with anodized aluminum oxide films. J Chem Phys. 126:2007;044701.
[49] Fennell CJ and Gezelter JD. Is the Ewald summation still necessary? Pairwise alternatives to the accepted standard for long-range electrostatics. J Chem Phys. 124:2006;234104.
[50] Hansen J, Schrøder T and Dyre J. Simplistic Coulomb forces in molecular dynamics: comparing the Wolf and shifted-force approximations. J Phys Chem B. 116:2012;5738.
[51] Irving J and Kirkwood J. The statistical mechanical theory of transport processes. IV. The equations of hydrodynamics. J Chem Phys. 18:1950;817.
[52] Todd B and Daivis P. Nonequilibrium molecular dynamics. Cambridge: Cambridge University Press; 2017.
[53] Mairhofer J and Sadus RJ. Thermodynamic properties of supercritical n–m Lennard-Jones fluids and isochoric and isobaric heat capacity maxima and minima. J Chem Phys. 139:2013;154503.